



The effect of TiO₂-coating layer on the performance in nanoporous ZnO-based dye-sensitized solar cells

Chohui Kim, Jongmin Kim, Hongsik Choi, Changwoo Nahm, Suji Kang, Sungjun Lee, Byungho Lee, Byungwoo Park*

WCU Hybrid Materials Program, Department of Materials Science and Engineering, Research Institute of Advanced Materials, Seoul National University, Seoul 151-744, Republic of Korea

HIGHLIGHTS

- Correlation between photovoltaic properties and TiO₂-coating thicknesses.
- Suppression of Zn²⁺/dye-complex formation and carrier recombination.
- Enhancement of power-conversion efficiency by a factor of three.

ARTICLE INFO

Article history:

Received 21 November 2012

Received in revised form

6 January 2013

Accepted 8 January 2013

Available online 16 January 2013

Keywords:

Dye-sensitized solar cells

Zinc oxide electrode

Titanium dioxide coating

Zinc–dye complex

ABSTRACT

Polydisperse ZnO spheres consisting of ~43-nm-sized nanoparticles are facily synthesized for dye-sensitized solar cells. A uniform TiO₂-coating layer on the ZnO surface improves both the open-circuit voltage and short-circuit current, and the power-conversion efficiency is consequently enhanced by a factor of approximately three. A thin coating layer suppresses the formation of Zn²⁺/dye complexes due to the enhanced chemical stability against the acidic dye, and also reduces charge recombination at the ZnO/dye/electrolyte interface.

© 2013 Elsevier B.V. All rights reserved.

1. Introduction

Dye-sensitized solar cells (DSSCs) have been regarded as potential candidates for next-generation solar cells due to their low cost, high durability, large flexibility in shape, and transparency [1–3]. While TiO₂ is the most commonly used oxide semiconductor, ZnO has also been considered as a promising candidate for DSSCs. The main reasons are carrier mobility of single-crystal ZnO (115–155 cm² V^{−1} s^{−1}), which is 2 orders of magnitude higher than that in TiO₂ (1–4 cm² V^{−1} s^{−1}), its direct bandgap (~3.2 eV), and the position of the conduction band similar to that of TiO₂ [4–8]. Furthermore, various ZnO nanostructures can be obtained by easy and low-cost techniques [9–18]. Despite these advantages, the performances of ZnO-based DSSCs are typically lower (7.5% as

a world record) [19] than those of TiO₂-based DSSCs (12.3% as a world record) [3]. The limited performance may be explained by the formation of Zn²⁺/dye complexes and recombination at the ZnO/dye/electrolyte interface [20,21]. The Zn²⁺/dye complexes are attributed to the poor chemical stability of ZnO in acidic dye solution, and are responsible for the inefficient electron injection from dye to semiconductor [22].

To overcome these problems, several coating layers such as Al₂O₃, MgO, Nb₂O₅, SiO₂, and TiO₂ have been studied [23–28]. Among these materials, TiO₂ has been attractive owing to its best performance in the optimized system with iodide-based electrolyte and organometallic dye. While TiO₂-coated ZnO electrodes have been reported by atomic-layer deposition (ALD) or corrosive TiCl₄ treatment [29–31], in this paper, a thin layer of TiO₂ is coated by a facile wet-chemical method that is inexpensive and noncorrosive. In addition, the involved mechanisms between the photovoltaic properties and TiO₂-coating thicknesses were identified in a nanoporous ZnO-based solar cell.

* Corresponding author. Tel.: +82 2 880 8319; fax: +82 2 885 9671.

E-mail address: byungwoo@snu.ac.kr (B. Park).

2. Experimental procedure

For the fabrication of polydisperse ZnO aggregates, zinc acetate dihydrate ($\text{Zn}(\text{CH}_3\text{COO})_2 \cdot 2\text{H}_2\text{O}$; Sigma–Aldrich) was added to diethylene glycol ($(\text{HOCH}_2\text{CH}_2)_2\text{O}$; Sigma–Aldrich), and heated in an autoclave at 160 °C for 6 h [32]. Then, the as-synthesized solution was centrifuged at 3000 rpm for 15 min, and dried at 60 °C. One gram of as-prepared ZnO powder, 0.45 g of cellulose ($(\text{C}_6\text{H}_{10}\text{O}_5)_n$; Aldrich), and 5 ml of terpeneol ($\text{C}_{10}\text{H}_{18}\text{O}$; Aldrich) were mixed, and stirred for one day. Terpeneol is an organic solvent with high boiling point and cellulose acts as a binder, preventing cracks during heat treatment and increasing adhesion among the ZnO nanospheres [33]. The resulting paste was spread on a fluorine-doped tin oxide substrate (FTO, TEC 8; Pilkington) by a doctor-blade method. The as-deposited films were subsequently annealed at 350 °C for 1 h.

The TiO_2 -coating layer on ZnO was prepared by a facile wet-chemical method. The as-prepared ZnO films were immersed in 10 mM titanium butoxide ($\text{Ti}[\text{O}(\text{CH}_2)_3\text{CH}_3]_4$; Aldrich) in 2-propanol ($(\text{CH}_3)_2\text{CHOH}$; Sigma–Aldrich) at room temperature (RT). The thickness of the coating layer was controlled by changing the deposition time (30, 60, and 120 min). The TiO_2 -coated films were post-annealed at 450 °C for 30 min, and the bare film was also sintered as a control set. After annealing, the films were sensitized with 0.5 mM of N719 dye ($\text{RuL}_2(\text{NCS})_2 \cdot 2\text{TBA}$, $L = 2,2'$ -bipyridyl-4,4'-dicarboxylic acid, TBA = tetrabutylammonium; Solaronix) for 6 h at RT, followed by rinsing with ethanol and drying under a nitrogen stream. To prepare the counter electrode, Pt thin film was deposited by rf-magnetron sputtering on the pre-drilled FTO substrate with two holes. The sensitized electrode and platinized counter electrode were sealed with thermoplastic foil (25 μm ; Dupont, U.S.A.), and the gap between the two electrodes was filled with an iodide-based redox electrolyte (AN-50; Solaronix, Switzerland).

The crystal structure of the electrode was analyzed by X-ray diffraction (XRD, M18XHF-SRA; MAC Science, Japan). Field-emission scanning electron microscopy (FE-SEM, SU70; Hitachi, Japan) was carried out to observe the morphology of the nanostructures. The photocurrent–voltage (J – V) curves were obtained on a solar cell measurement system (K3000; McScience, Korea) under a solar simulator (Xenon lamp, air mass (AM) 1.5, 100 mW cm^{-2}). High-resolution transmission electron microscopy

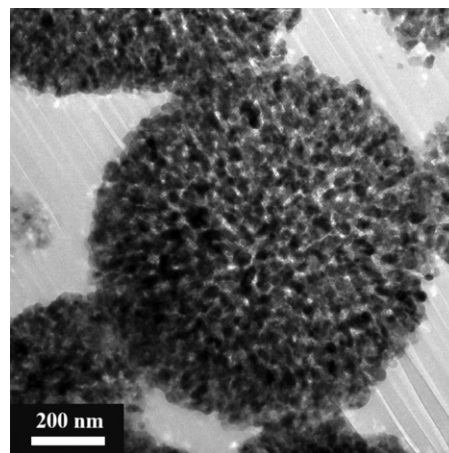


Fig. 2. Cross-sectional TEM image of nanoporous ZnO spheres coated with TiO_2 (60 min).

(HRTEM, JEM-3000F; JEOL, Japan) and a focused ion beam (FIB, SMI3050SE; SII Nanotechnology Inc., Japan) were used to identify the uniform coating of TiO_2 through the nanoporous ZnO spheres. The elemental compositions and distribution were examined using energy-dispersive X-ray spectroscopy (EDX, ISIS-300; Oxford Instruments). An inductively coupled plasma-atomic emission spectrometer (ICP-AES, Optima-4300 DV; Perkin–Elmer, MA, U.S.A.) was employed to determine the atomic ratio of Ti/Zn in the electrode. In order to investigate the electrochemical reactions at the interfaces [34–36], electrochemical impedance spectroscopy (EIS) and open-circuit voltage decay (OCVD) were measured from a potentiostat (CHI 608C; CH Instrumental Inc., Austin, U.S.A.). The absorption spectra of the unloaded dye molecules were recorded on a UV/Vis spectrophotometer (Lambda 20; Perkin–Elmer, Waltham, U.S.A.), and incident photon-to-current conversion efficiency (IPCE) spectra were measured on an IPCE measurement system (K3100; McScience, Korea).

3. Results and discussion

To clearly identify the mechanisms of the TiO_2 -coating layers with various thicknesses, the experiment was performed with

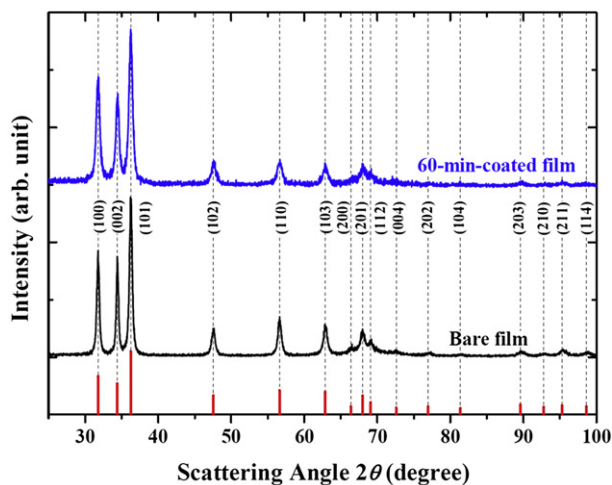


Fig. 1. X-ray diffraction of bare and 60-min-coated film after 450 °C annealing. The peak intensities and positions from the hexagonal ZnO (JCPDS #36-1451) are shown as solid lines.

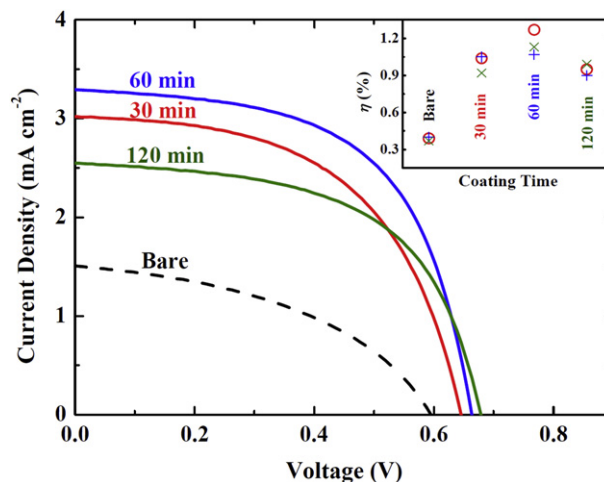


Fig. 3. Photocurrent–voltage curves of DSSCs with various TiO_2 -coating times, and the inset shows the corresponding power-conversion efficiency (dye-adsorption time: 6 h).

Table 1

Performance of DSSCs consisting of nanoporous ZnO spheres with various TiO₂-coating times (dye-adsorption time: 6 h).

| | J_{sc} (mA cm ⁻²) | V_{oc} (V) | FF | η |
|---------|---------------------------------|--------------|-------|--------|
| Bare | 1.50 | 0.595 | 43.9% | 0.39% |
| 30 min | 3.02 | 0.645 | 54.2% | 1.06% |
| 60 min | 3.30 | 0.663 | 58.3% | 1.27% |
| 120 min | 2.55 | 0.679 | 57.2% | 0.99% |

extremely long dye-adsorption time (6 h). The most critical reason for the low efficiency of ZnO-based DSSCs is the formation of Zn²⁺/dye complexes. When ZnO is immersed in acidic dye solution, the dissolved Zn²⁺ ions and deprotonated dyes form Zn²⁺/dye complexes [22]. These complexes cover the surface as a multilayer form, and change the original morphology of the electrode. Furthermore, they can absorb the visible light, and the electron transfer through these complexes is not effective [21]. The Zn²⁺/dye-complex formation is much severe under the extreme condition (6 h), and the suppressed complex formation by TiO₂-coating layer can be observed more dramatically. To achieve higher efficiency, shorter immersion time (30 min) is also performed, since typical ZnO-based DSSCs exhibit approximately 1.5%–5.4% [32,37–40].

The ZnO nanoparticle has hexagonal wurtzite structure (JCPDS #36-1451), with no zinc-blende phase (JCPDS #77-0191), and TiO₂ is not detected due to the subnanometer-scale coating (XRD analysis in Fig. 1). Grain size is obtained from the Williamson–Hall plot [41], and that of 60-min-coated film after 450 °C annealing is ~43 nm, consistent with the cross-sectional TEM image of Fig. 2. The nanocrystallites are able to provide relatively large surface area, and the submicrometer-sized particles can provide effective light scattering [19,32].

The TiO₂-coating layer on the ZnO surface improves both the open-circuit voltage (V_{oc}) and short-circuit current (J_{sc}), as shown in the J – V curves of Fig. 3. In particular, the 60-min-coated cell shows an optimum power-conversion efficiency of 1.27%, an increase by a factor of three compared with that of the bare cell. As the coating

layer becomes thicker, V_{oc} gradually increases while J_{sc} decreases, as summarized in Table 1.

The nanoparticle size of the bare film without TiO₂ coating (Fig. 4(a)) is bigger than that of the coated film after 450 °C annealing (Fig. 4(c)), indicating that the TiO₂-coating layer inhibits the coarsening behavior of ZnO nanoparticles (before dye loading) [42]. This is also supported by the larger full-width at half-maximum (FWHM) of the coated film from diffraction (Fig. 1) [43,44]. Therefore, 60-min-coated film has relatively large surface area. After dye loading, the bare film (Fig. 4(b)) is covered with Zn²⁺/dye complexes. However, no significant morphological change is observed in the coated film, confirming that the TiO₂ layer efficiently restrains the formation of Zn²⁺/dye complexes.

Fig. 5 confirms the homogeneous coating of TiO₂, from the spatial distribution of Zn and Ti elements throughout the nanopores. With the atomic ratios of Ti/Zn measured by ICP-AES, the coating thickness is in the subnanometer range if assumed uniform coating. Most of the generated electron carriers from dye would transfer through the ZnO nanoparticles because TiO₂ layer is too thin to transfer electrons effectively, and also ZnO is a preferred electron channel due to the high mobility [4,5]. The detailed description about the thickness calculation is provided in the supplemental materials (Table S1).

The amount of dye in the DSSCs was measured by UV–visible absorption, as shown in Fig. 6, considering the molar absorption coefficient of N719 dye ($\sim 10^4$ M⁻¹ cm⁻¹ at 543 nm) [45]. While the dye loading of all the coated films is higher than that of the bare film, the 60-min-coated film shows the optimum value. The increase in dye loading is attributed to the suppression of Zn²⁺/dye-complex formation at the outer surface of ZnO sphere, which can block the dye diffusion into the nanoporous sphere. In the 120-min-coated film, the amount of dye is slightly decreased. A possible reason is the loss of surface area due to the coating on the nanoporous connections among ZnO nanoparticles.

Impedance analysis was performed at the open-circuit condition under AM 1.5 [46–48], and the resistance (between $\sim 10^0$ and $\sim 10^3$ Hz) increases with the thickness of the coating layer (Fig. 7).

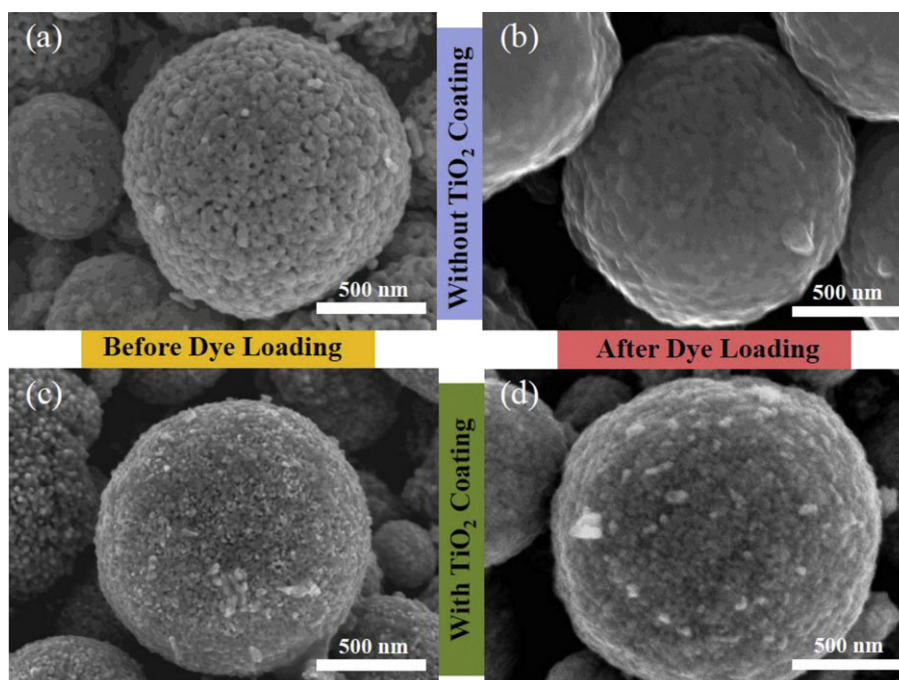


Fig. 4. Plan-view FE-SEM images of nanoporous ZnO spheres with/without TiO₂-coating layer (60 min) followed by 450 °C annealing, and before/after dye loading.

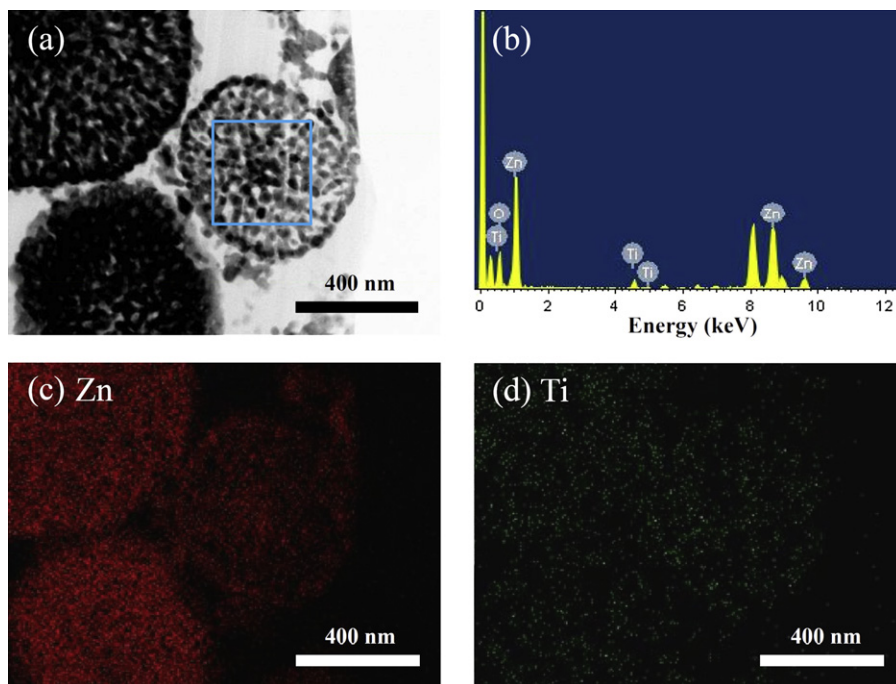


Fig. 5. (a) Cross-sectional TEM image of nanoporous ZnO spheres (60-min-coated film), (b) elemental analysis, and (c and d) EDX mapping of Zn and Ti, respectively.

This indicates that the TiO_2 -coating layer suppresses back electron transfer, and consequentially improves V_{oc} [49,50]. Thicker coating, however, also suppresses forward electron injection, resulting in a decreased current density [51–54]. The bare cell shows the highest resistance due to the formation of resistive Zn^{2+} /dye complexes.

Reduction of charge recombination was also observed (Fig. 8) [55–57]. The decay response of the coated cell is slower than that of the bare cell, indicating that recombination is effectively reduced. The electron-carrier lifetime (τ) is obtained from Ref. [55]:

$$\tau = -\frac{k_B T}{e} \left(\frac{dV_{oc}}{dt} \right)^{-1}, \quad (1)$$

where $k_B T$ is the thermal energy, e is the elementary charge, and t is time (Fig. 8(b)). The electron-carrier lifetime of the coated cell is

approximately one order of magnitude higher in comparison with the bare cell.

The TiO_2 -coated cells show higher IPCE values than the bare cell in the whole visible region due to the reduction of recombination by TiO_2 coating, as shown in Fig. 9. Even in the lower wavelength region (below ~ 390 nm) where light is mainly absorbed by ZnO, the IPCE of the bare cell is still lower than that of the coated cell because of the formation of Zn^{2+} /dye complexes, while the degree of enhancement among the coated cells becomes insignificant. The bandgap of ZnO nanoparticle aggregate is expected to be similar to that of the bulk (~ 3.2 eV), because the size of nanoparticle (~ 43 nm) is much larger than the excitonic diameter of ZnO (~ 5.6 nm) [58]. The IPCE value dropped to zero at wavelength around 300 nm due to the absorption of FTO [59].

The shorter dye-adsorption time (30 min) is also performed for higher efficiency, and the corresponding photocurrent density–voltage (J – V) characteristics are presented in Fig. 10. These results

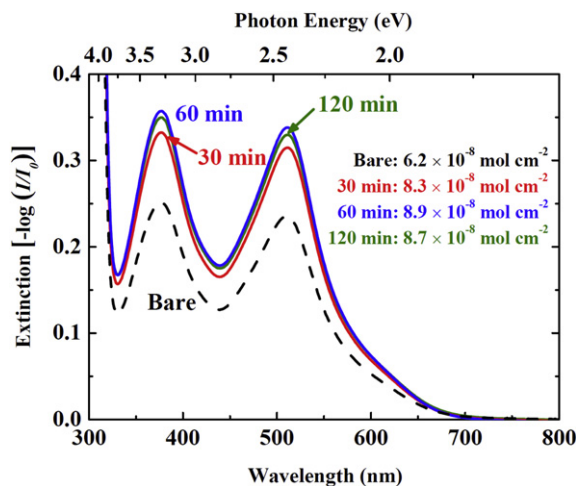


Fig. 6. UV–Vis absorption spectra of N719 desorbed from DSSCs in 1 M NaOH solution.

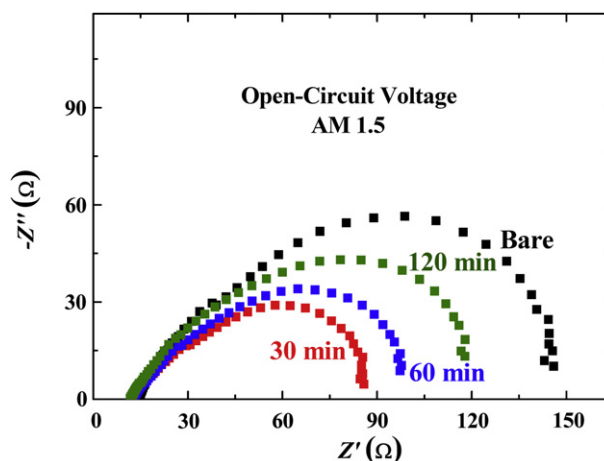


Fig. 7. Nyquist plots with different coating times.

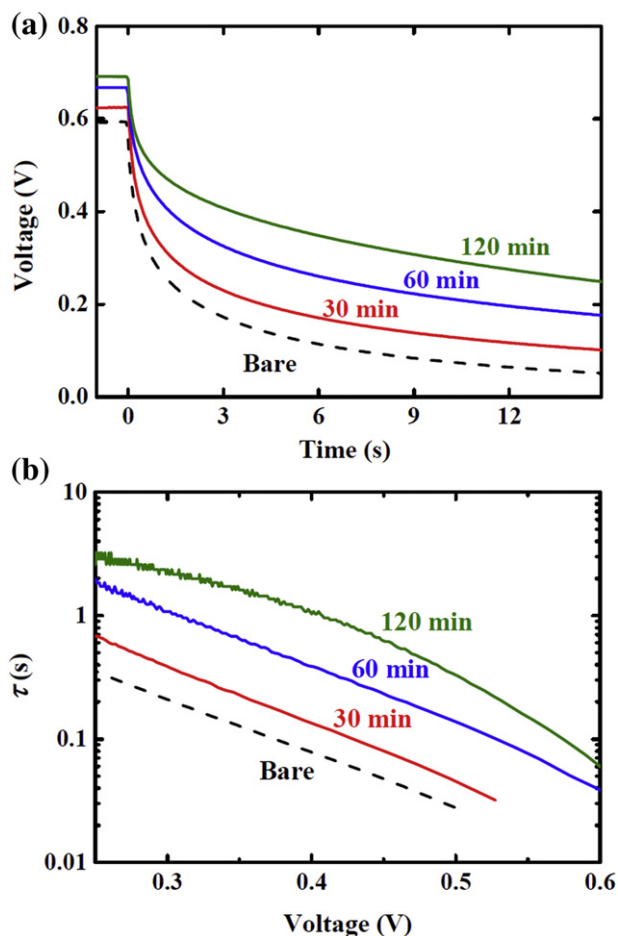


Fig. 8. (a) Experimental decay results of V_{oc} for the bare and coated cells. (b) Electron lifetime from Eq. (1) as a function of voltage.

indicate similar tendency with that of the longer dye-immersion time (6 h) that V_{oc} increases while J_{sc} decreases, as the coating-layer thickness increases (Table 2). The optimum power-conversion efficiency of 2.54% is obtained in the 60-min-coated

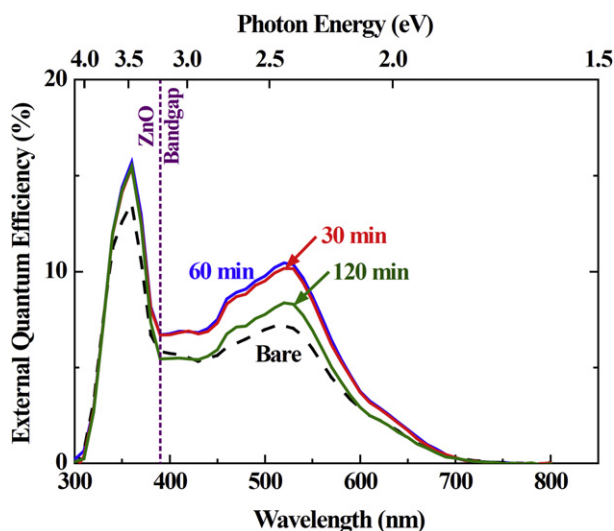


Fig. 9. Incident photon-to-current conversion efficiency (IPCE) spectra of bare and coated cells.

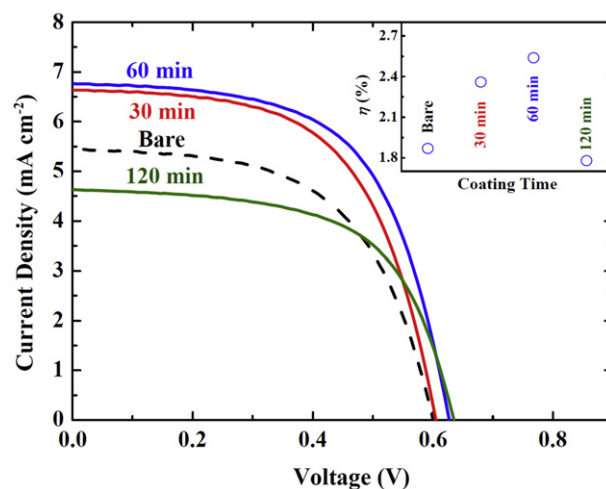


Fig. 10. Photocurrent density–voltage characteristics of the TiO_2 -coated ZnO-based DSSCs (dye-adsorption time: 30 min), and the inset shows the power-conversion efficiency of DSSCs with respect to the TiO_2 -coating time.

Table 2

Short-circuit current, open-circuit voltage, fill factor, and power-conversion efficiency of the DSSCs with various TiO_2 -coating times (dye-adsorption time: 30 min).

| | J_{sc} (mA cm^{-2}) | V_{oc} (V) | FF | η |
|---------|----------------------------------|--------------|-------|--------|
| Bare | 5.44 | 0.601 | 57.2% | 1.87% |
| 30 min | 6.64 | 0.605 | 58.7% | 2.36% |
| 60 min | 6.77 | 0.627 | 59.9% | 2.54% |
| 120 min | 4.63 | 0.635 | 60.4% | 1.78% |

cell, which is $\sim 26\%$ higher than that of the bare cell (1.87%). The interface stability of TiO_2 -coated cell is investigated for two weeks, as shown in Fig. 11. In the first several days, both V_{oc} and fill factor (FF) increase while J_{sc} decreases, resulting in the 15% decrease in efficiency. The former may be attributed to adsorption of electrolyte additives on the electrode surface, and the latter may result from the dissolution of Zn into the electrolyte [60,61]. The efficiency, however, remains relatively constant after several days, indicating good stability of the interfaces. Schematic representations illustrate the effect of the TiO_2 -coating layer (Fig. 12). This coating layer not only reduces the recombination and formation of Zn^{2+} /dye complexes, but also preserves the relatively large surface area. These

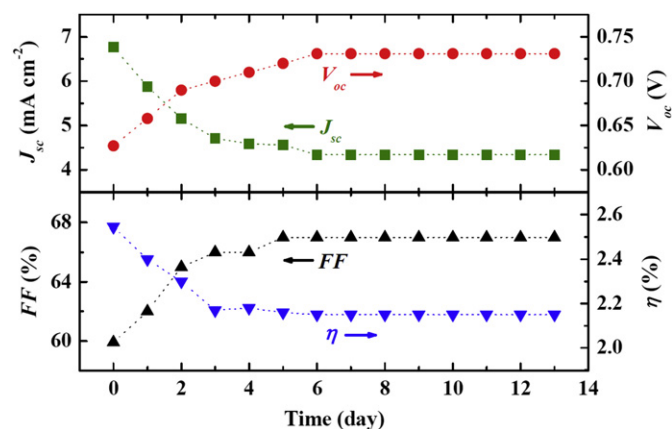


Fig. 11. The changes of short-circuit current, open-circuit voltage, fill factor, and power-conversion efficiency of the 60-min-coated cell for two weeks (dye-adsorption time: 30 min).

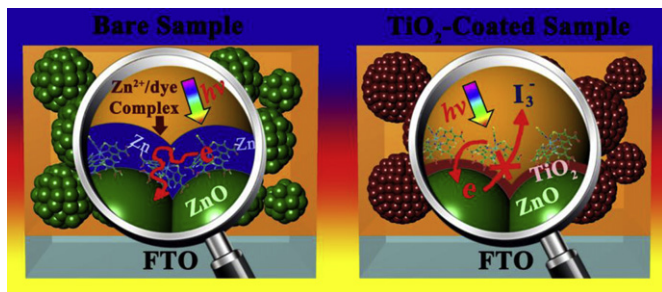


Fig. 12. Schematic figures for the effect of TiO_2 -coating layer on the performance of ZnO-based dye-sensitized solar cells.

results directly influence the improved V_{oc} , J_{sc} , and FF compared with the bare cell.

4. Conclusions

The effect of TiO_2 -coating layers on the performance of ZnO-based DSSCs is systematically investigated with various TiO_2 -coating thicknesses. The TiO_2 layers play an important role in the suppression of the formation of Zn^{2+} /dye complexes and recombination at the ZnO/dye/electrolyte interface. As a result, the power-conversion efficiency is enhanced by a factor of approximately three.

Acknowledgments

This research was supported by the National Research Foundation of Korea, through the World Class University (WCU, R31-2008-000-10075-0) and the Korean Government (MEST: NRF, 2010-0029065).

Appendix A. Supplementary data

Supplementary data related to this article can be found at <http://dx.doi.org/10.1016/j.jpowsour.2013.01.042>.

References

- [1] B. O'Regan, M. Grätzel, *Nature* 353 (1991) 737–740.
- [2] J.M. Kroon, N.J. Bakker, H.J.P. Smit, P. Liska, K.R. Thampi, P. Wang, S.M. Zakeeruddin, M. Grätzel, A. Hinsch, S. Hore, U. Würfel, R. Sastrawan, J.R. Durrant, E. Palomares, H. Pettersson, T. Gruszecki, J. Walter, K. Skupien, G.E. Tulloch, *Prog. Photovoltaics* 15 (1) (2007) 1–18.
- [3] A. Yella, H.W. Lee, H.N. Tsao, C. Yi, A.K. Chandiran, M.K. Nazeeruddin, E.W.G. Diau, C.Y. Yeh, S.M. Zakeeruddin, M. Grätzel, *Science* 334 (2011) 629–634.
- [4] E.M. Kaidashev, M. Lorenz, H. Wenckstern, A. Rahm, H.C. Semmelhack, K.H. Han, G. Benndorf, C. Bundesmann, H. Hochmuth, M. Grundmann, *Appl. Phys. Lett.* 82 (2003) 3901–3903.
- [5] E. Hendry, F. Wang, J. Shan, T.F. Heinz, M. Bonn, *Phys. Rev. B* 69 (2004) 081101.
- [6] H. Tang, K. Prasad, R. Sanjinès, P.E. Schmid, F. Lévy, *J. Appl. Phys.* 75 (1994) 2042–2047.
- [7] K. Keis, L. Vayssieres, H. Rensmo, S.E. Lindquist, A. Hagfeldt, *J. Electrochem. Soc.* 148 (2001) A149–A155.
- [8] S.M. Prokes, J.L. Gole, X.B. Chen, C. Burda, W.E. Carlos, *Adv. Funct. Mater.* 15 (2005) 161–167.
- [9] E. Meulenkaamp, *J. Phys. Chem. B* 102 (1998) 5566–5572.
- [10] S. Kar, A. Dev, S. Chaudhuri, *J. Phys. Chem. B* 110 (2006) 17848–17853.
- [11] Q.C. Li, V. Kumar, Y. Li, H.T. Zhang, T.J. Marks, R.P.H. Chang, *Chem. Mater.* 17 (2005) 1001–1006.
- [12] X.D. Wang, Y. Ding, C.J. Summers, Z.L. Wang, *J. Phys. Chem. B* 108 (2004) 8773–8777.
- [13] M. Fu, J. Zhou, Q.F. Xiao, B. Li, R.L. Zong, W. Chen, J. Zhang, *Adv. Mater.* 18 (2006) 1001–1004.
- [14] Z.L. Wang, *J. Phys. Condens. Matter* 16 (2004) R829–R858.
- [15] M. Vafaei, M.S. Ghamsari, *Mater. Lett.* 61 (2007) 3265–3268.
- [16] P.D. Yang, H.Q. Yan, S. Mao, R. Russo, J. Johnson, R. Saykally, N. Morris, J. Pham, R.R. He, H.J. Choi, *Adv. Funct. Mater.* 12 (2002) 323–331.
- [17] K. Nonomura, T. Yoshida, D. Schlettwein, H. Minoura, *Electrochim. Acta* 48 (2003) 3071–3078.
- [18] H.H. Wang, C.S. Xie, *J. Cryst. Growth* 291 (2006) 187–195.
- [19] N. Memarian, I. Concina, A. Braga, S.M. Rozati, A. Vomiero, G. Sberveglieri, *Angew. Chem. Int. Ed.* 50 (2011) 12317–12337.
- [20] N.A. Anderson, X. Ai, T.J. Lian, *J. Phys. Chem. B* 107 (2003) 14414–14421.
- [21] K. Keis, J. Lindgren, S.E. Lindquist, A. Hagfeldt, *Langmuir* 16 (2000) 4688–4694.
- [22] H. Horiuchi, R. Katoh, K. Hara, M. Yanagida, S. Murata, H. Arakawa, M. Tachiya, *J. Phys. Chem. B* 107 (2003) 2570–2574.
- [23] J.C. Guo, C.X. She, T.Q. Lian, *J. Phys. Chem. C* 111 (2007) 8979–8987.
- [24] E. Palomares, J.N. Clifford, S.A. Haque, T. Lutz, J.R. Durrant, *J. Am. Chem. Soc.* 125 (2003) 475–482.
- [25] S. Wu, H.W. Han, Q.D. Tai, J. Zhang, S. Xu, C.H. Zhou, Y. Yang, H. Hu, B.L. Chen, B. Sebo, X.Z. Zhao, *Nanotechnology* 19 (2008) 215704.
- [26] S.G. Chen, S. Chappel, Y. Diamant, A. Zaban, *Chem. Mater.* 13 (2001) 4629–4634.
- [27] Y.J. Shin, J.H. Lee, J.H. Park, N.G. Park, *Chem. Lett.* 36 (2007) 1506–1507.
- [28] D.B. Menzies, Q. Dai, L. Bourgeois, R.A. Caruso, Y.B. Cheng, G.P. Simon, L. Spiccia, *Nanotechnology* 18 (2007) 125608.
- [29] K. Park, Q. Zhang, B.B. Garcia, X. Zhou, Y.H. Jeong, G. Cao, *Adv. Mater.* 22 (2010) 1–5.
- [30] P. Atienzar, T. Ishwara, B.N. Illy, M.P. Ryan, B.C. O'Regan, J.R. Durrant, J. Nelson, *J. Phys. Chem. Lett.* 1 (2008) 708–713.
- [31] N. Sakai, N. Kawashima, T.N. Murakami, *Chem. Lett.* 40 (2011) 162–164.
- [32] Q. Zhang, T.P. Chou, B. Russo, S.A. Jenekhe, G. Cao, *Angew. Chem. Int. Ed.* 47 (2008) 2402–2406.
- [33] H. Li, Z. Xie, Y. Zhang, J. Wang, *Thin Solid Films* 518 (2010) E68–E71.
- [34] Y. Park, B. Lee, C. Kim, J. Kim, S. Nam, Y. Oh, B. Park, *J. Phys. Chem. C* 114 (2010) 3688–3692.
- [35] B. Kim, C. Kim, T.G. Kim, D. Ahn, B. Park, *J. Electrochem. Soc.* 153 (2006) A1773–A1777.
- [36] J. Cho, Y.W. Kim, B. Kim, J.G. Lee, B. Park, *Angew. Chem. Int. Ed.* 42 (2003) 1618–1621.
- [37] A.B.F. Martinson, J.W. Elam, J.T. Hupp, M.J. Pellin, *Nano Lett.* 7 (2007) 2183–2187.
- [38] M. Saito, S. Fujihara, *Energy Environ. Sci.* 1 (2008) 280–283.
- [39] S.B. Ambadea, R.S. Mane, S.H. Han, S.H. Lee, M.M. Sung, O.S. Joo, *J. Photochem. Photobiol. A* 222 (2011) 366–369.
- [40] S. Yodyingyong, Q. Zhang, K. Park, C.S. Dandaneau, X. Zhou, D. Triampo, G. Cao, *Appl. Phys. Lett.* 96 (2010) 073115.
- [41] C. Suryanarayana, M.G. Norton, *X-ray Diffraction: A Practical Approach* (1998). New York.
- [42] K. Park, Q. Zhang, B.B. Garcia, G. Cao, *J. Phys. Chem. C* 115 (2011) 4927–4934.
- [43] T. Moon, S. Hwang, D. Jung, D. Son, C. Kim, J. Kim, M. Kang, B. Park, *J. Phys. Chem. C* 111 (2007) 4164–4167.
- [44] J.L. Gole, S.M. Prokes, O.J. Glembocki, *J. Phys. Chem. C* 112 (2008) 1782–1788.
- [45] J.D.J. Ingle, S.R. Crouch, *Spectrochemical Analysis* (1988). New Jersey.
- [46] B. Yoo, K.J. Kim, S.Y. Bang, M.J. Ko, K. Kim, N.G. Park, *J. Electroanal. Chem.* 638 (2010) 161–166.
- [47] H. Choi, C. Nahm, J. Kim, J. Moon, S. Nam, C. Kim, D.-R. Jung, B. Park, *Curr. Appl. Phys.* 12 (2012) 737–741.
- [48] J. Kim, H. Choi, C. Nahm, C. Kim, S. Nam, S. Kang, D.-R. Jung, J.I. Kim, J. Kang, B. Park, *J. Power Sources* 220 (2012) 108–113.
- [49] C.H. Lin, S. Chattopadhyay, C.W. Hsu, M.H. Wu, W.C. Chen, C.T. Wu, S.C. Tseng, J.S. Hwang, J.H. Lee, C.W. Chen, C.H. Chen, L.C. Chen, K.H. Chen, *Adv. Mater.* 21 (2009) 759–763.
- [50] L. Larina, D. Shin, J.H. Kim, B.T. Ahn, *Energy Environ. Sci.* 4 (2011) 3487–3493.
- [51] S.W. Boettcher, E.L. Warren, M.C. Putnam, E.A. Santori, D. Turner-Evans, M.D. Kelzenberg, M.G. Walter, J.R. McKone, B.S. Brunschwig, H.A. Atwater, N.S. Lewis, *J. Am. Chem. Soc.* 133 (2011) 1216–1219.
- [52] A. Irannejad, K. Janghorban, O.K. Tan, H. Huang, C.K. Lim, P.Y. Tan, X. Fang, C.S. Chua, S. Maleksaeedi, S.M.H. Hejazi, M.M. Shahjamali, M. Ghaffari, *Electrochim. Acta* 58 (2011) 19–24.
- [53] M. Law, L.E. Greene, A. Radenovic, T. Kuykendall, J. Liphardt, P. Yang, *J. Phys. Chem. B* 110 (2006) 22652–22663.
- [54] A. Mihi, C. Zhang, P.V. Braun, *Angew. Chem. Int. Ed.* 50 (2011) 5712–5715.
- [55] A. Zaban, M. Greenshtein, J. Bisquert, *ChemPhysChem* 4 (2003) 859–864.
- [56] J. Bisquert, A. Zaban, M. Greenshtein, I. Mora-Seró, *J. Am. Chem. Soc.* 126 (2004) 13550–13559.
- [57] J. Kim, H. Choi, C. Nahm, J. Moon, C. Kim, S. Nam, D.-R. Jung, B. Park, *J. Power Sources* 196 (2011) 10526–10531.
- [58] R. Viswanatha, S. Sapra, B. Satpati, P.V. Satyam, B.N. Dev, D.D. Sarma, *J. Mater. Chem.* 14 (2004) 661–668.
- [59] X.Z. Guo, Y.D. Zhang, Y.H. Qin, Y.H. Luo, D.M. Li, Y.T. Pang, Q.B. Meng, *J. Power Sources* 195 (2010) 7684–7690.
- [60] L. Ke, S.B. Dolmanan, L. Shen, P.K. Pallathadk, Z. Zhang, D.M. Lai, H. Liu, *Sol. Energy Mater. Sol. Cells* 94 (2010) 323–326.
- [61] R. Katoh, M. Kasuya, S. Kodate, A. Furube, N. Koide, *J. Phys. Chem. C* 113 (2009) 20738–20744.